

Intrinsic piezoelectricity in monolayer XSi_2N_4 ($\text{X}=\text{Ti}, \text{Zr}, \text{Hf}, \text{Cr}, \text{Mo}$ and W)

San-Dong Guo^{1,2}, Yu-Tong Zhu¹ and Wen-Qi Mu¹

¹*School of Electronic Engineering, Xi'an University of Posts and Telecommunications, Xi'an 710121, China and*

²*Key Laboratory of Advanced Semiconductor Devices and Materials, Xi'an University of Posts and Telecommunications, Xi'an 710121, China*

Motivated by experimentally synthesized MoSi_2N_4 (*Science* 369, 670-674 (2020)), the intrinsic piezoelectricity in monolayer XSi_2N_4 ($\text{X}=\text{Ti}, \text{Zr}, \text{Hf}, \text{Cr}, \text{Mo}$ and W) are studied by density functional theory (DFT). Among the six monolayers, the CrSi_2N_4 has the best piezoelectric strain coefficient d_{11} of 1.24 pm/V, and the second is 1.15 pm/V for MoSi_2N_4 . Taking MoSi_2N_4 as an example, strain engineering is applied to improve d_{11} . It is found that tensile biaxial strain can enhance d_{11} of MoSi_2N_4 , and the d_{11} at 4% can improve by 107% with respect to unstrained one. By replacing the N by P or As in MoSi_2N_4 , the d_{11} can be raise substantially. For MoSi_2P_4 and MoSi_2As_4 , the d_{11} is as high as 4.93 pm/V and 6.23 pm/V, which is mainly due to smaller $C_{11} - C_{12}$ and very small minus or positive ionic contribution to piezoelectric stress coefficient e_{11} with respect to MoSi_2N_4 . The discovery of this piezoelectricity in monolayer XSi_2N_4 enables active sensing, actuating and new electronic components for nanoscale devices, and is recommended for experimental exploration.

PACS numbers: 71.20.-b, 77.65.-j, 72.15.Jf, 78.67.-n
Keywords: MoSi_2N_4 , Piezoelectronics, 2D materials

Email:sandongyuwang@163.com

I. INTRODUCTION

Piezoelectric materials can convert mechanical energy into electrical energy and vice versa, and the piezoelectricity of two-dimensional (2D) materials has been widely investigated¹ in recent years. Experimentally, the existence of piezoelectricity of MoS_2 ^{2,3}, MoSSe ⁴ and In_2Se_3 ⁵ has significantly promoted development of the piezoelectricity of 2D materials. It has been reported that a large number of 2D materials have significant piezoelectric coefficients, such as transition metal dichalcogenides (TMD), Janus TMD, group IIA and IIB metal oxides, group-V binary semiconductors and group III-V semiconductors⁶⁻¹⁵, the monolayer SnSe , SnS , GeSe and GeS of which possess giant piezoelectricity, as high as 75-251 pm/V¹². Due to different crystal symmetry, a only in-plane piezoelectricity, both in-plane and out-of-plane piezoelectricity, or a pure out-of-plane piezoelectricity can exit, and the corresponding example is TMD monolayers¹¹, many 2D Janus materials^{6,9} and pentagraphene¹⁰. The strain-tuned piezoelectric response of MoS_2 ¹⁶, AsP ⁷, SnSe ⁷ and Janus TMD monolayers¹⁷ have been performed by the first-principle calculations, and it is proved that strain can improve the piezoelectric strain coefficients.

Recently, the layered 2D MoSi_2N_4 has been synthesized by chemical vapor deposition (CVD)¹⁸. Many other 2D materials with a general formula of XY_2M_4 have been predicted by DFT calculations¹⁸, where X represents an early transition metal (W, V, Nb, Ta, Ti, Zr, Hf, or Cr), Y is Si or Ge, and M stands for N, P, or As. In this work, the piezoelectric properties of monolayer XSi_2N_4 ($\text{X}=\text{Ti}, \text{Zr}, \text{Hf}, \text{Cr}, \text{Mo}$ and W) are studied by using density functional perturbation theory (DFPT)¹⁹. The independent in-plane piezoelectric constants d_{11} is predicted to be 0.777 pm/V to 1.241 pm/V, which are smaller than ones of many other 2D materials^{6,9,11-13}. Using MoSi_2N_4 as

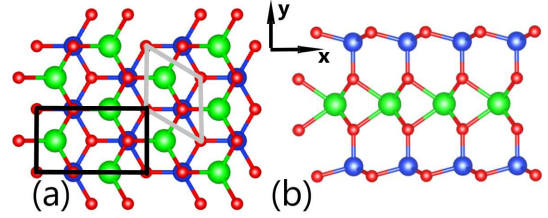


FIG. 1. (Color online)The crystal structure of monolayer XSi_2N_4 , including (a) top view and (b) side view. The primitive cell is marked by gray line, and the rectangle supercell is marked by black line to calculate piezoelectric coefficients. The large green balls represent X atoms, and the middle blue balls for Si atoms, and the small red balls for N atoms.

an example, strain engineering is proposed to produce improved piezoelectric properties. It is found that increasing strain can improve d_{11} due to reduced $C_{11}-C_{12}$ and enhanced e_{11} , and the band gap decreases. Calculated results show that MoSi_2P_4 and MoSi_2As_4 have more better d_{11} than XSi_2N_4 ($\text{X}=\text{Ti}, \text{Zr}, \text{Hf}, \text{Cr}, \text{Mo}$ and W), which is mainly because they are more softer, and their ionic parts have very small minus contribution (MoSi_2P_4) or positive contribution (MoSi_2As_4) to e_{11} . Our calculations show that the XY_2M_4 ($\text{X}=\text{Ti}, \text{Zr}, \text{Hf}, \text{Cr}, \text{Mo}$ or W ; $\text{Y}=\text{Si}$ or Ge ; and $\text{M}=\text{N}, \text{P}$ or As) materials may be promising candidates for piezoelectric applications.

II. COMPUTATIONAL DETAIL

We perform DFT calculations²⁰ using the projector-augmented wave method as implemented in the plane-wave code VASP²¹⁻²³. For the structural relaxation and the calculations of the elastic and piezoelectric tensors, we use the popular generalized gradient approximation of Perdew, Burke and Ernzerhof (GGA-PBE)²⁴ as the

TABLE I. For monolayer XSi_2N_4 ($\text{X}=\text{Ti}, \text{Zr}, \text{Hf}, \text{Cr}, \text{Mo}$ and W), the lattice constants a_0 (\AA), the height h (\AA), the GGA gap Gap (eV), the GGA+SOC gap Gap_{soc} (eV), the spin-orbital splitting at K point Δ (eV), the elastic constants $C_{11}-C_{12}$ (Nm^{-1}), the piezoelectric coefficients e_{11} (10^{-10} C/m) and d_{11} (pm/V).

Name	a_0	h	Gap	Gap_{soc}	Δ	$C_{11}-C_{12}$	e_{11}	d_{11}
TiSi_2N_4	2.931	6.908	1.629	1.628	0.033	326.239	2.712	0.831
ZrSi_2N_4	3.032	7.035	1.629	1.625	0.056	287.008	2.229	0.777
HfSi_2N_4	3.022	7.000	1.802	1.789	0.183	303.898	3.199	1.053
CrSi_2N_4	2.844	6.869	0.498	0.499	0.063	358.021	4.442	1.241
MoSi_2N_4	2.909	7.004	1.747	1.746	0.130	383.982	4.398	1.145
WSi_2N_4	2.912	7.014	2.083	2.074	0.399	403.227	3.138	0.778

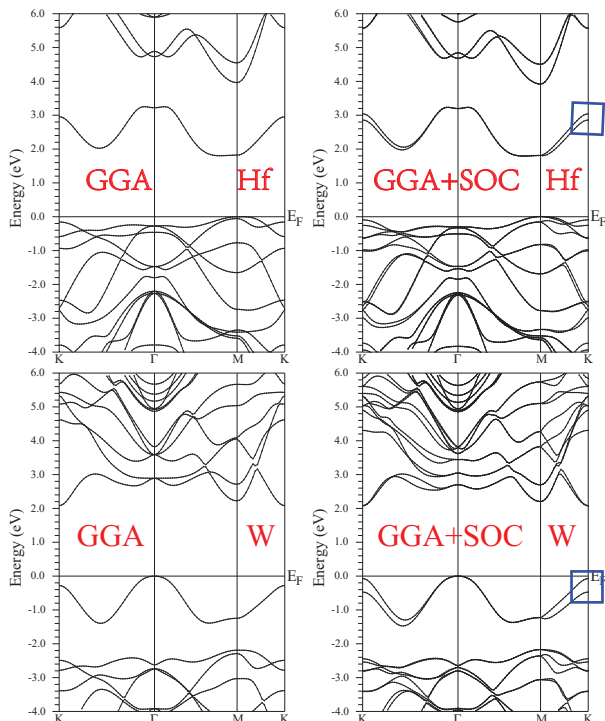


FIG. 2. (Color online) The GGA and GGA+SOC energy band structures of HfSi_2N_4 and WSi_2N_4 , and the spin-orbital splitting at K point is marked by the little blue box.

exchange-correlation functional. For energy band calculations, the spin orbital coupling (SOC) is also taken into account. A cutoff energy of 500 eV for the plane wave basis set is used to ensure an accurate DFT calculations. A vacuum spacing of more than 32 \AA is adopted to reduce the interactions between the layers, which is key to attain accurate e_{ij} . The total energy convergence criterion is set to 10^{-8} eV, and the Hellmann-Feynman forces on each atom are less than $0.0001 \text{ eV} \cdot \text{\AA}^{-1}$. The coefficients of the elastic stiffness tensor C_{ij} are calculated by using strain-stress relationship (SSR), and the piezoelectric stress coefficients e_{ij} are attained by DFPT method¹⁹. The Brillouin zone sampling is done using a Monkhorst-Pack mesh of $15 \times 15 \times 1$ for C_{ij} , and $9 \times 16 \times 1$ for e_{ij} . The 2D elastic coefficients C_{ij}^{2D} and piezoelec-

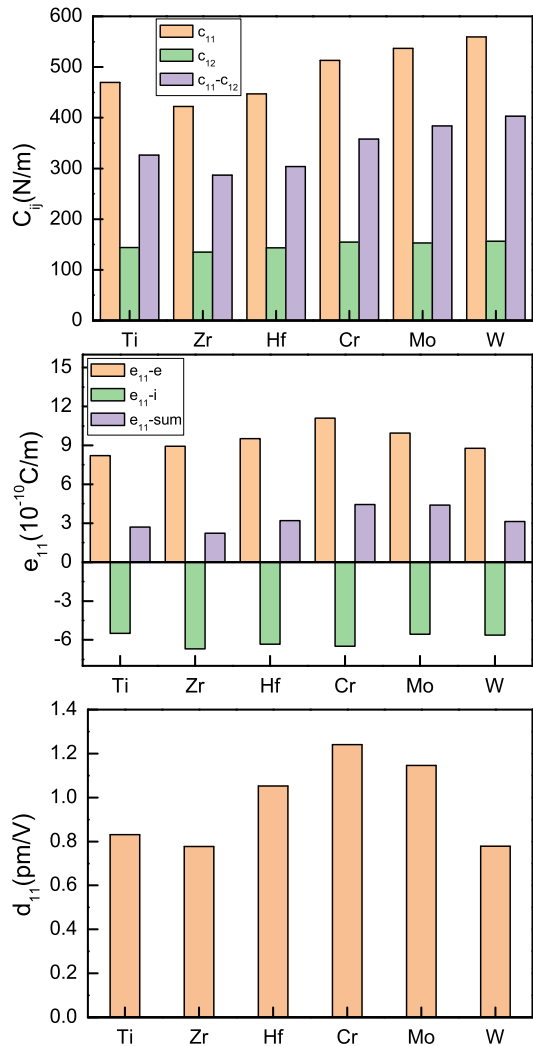


FIG. 3. (Color online) For XSi_2N_4 ($\text{X}=\text{Ti}, \text{Zr}, \text{Hf}, \text{Cr}, \text{Mo}$ and W): (Top) the elastic constants C_{ij} , (Middle) piezoelectric stress coefficients e_{11} and the ionic contribution and electronic contribution to e_{11} , and (Bottom) piezoelectric strain coefficients d_{11} .

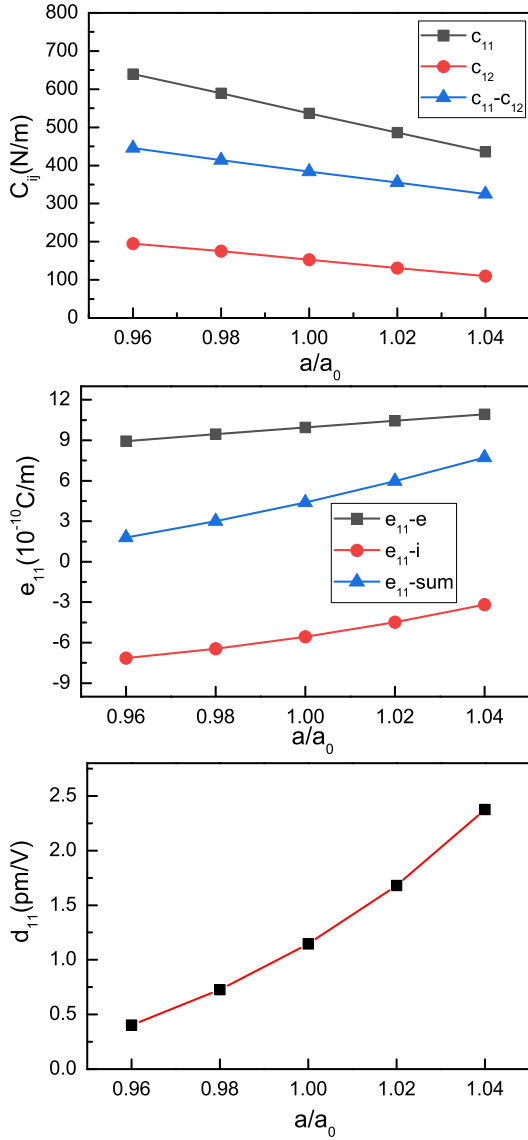


FIG. 4. (Color online) For experimentally achieved monolayer MoSi_2N_4 , (Top) the elastic constants C_{ij} , (Middle) piezoelectric stress coefficients e_{11} and the ionic contribution and electronic contribution to e_{11} , and (Bottom) piezoelectric strain coefficients d_{11} as a function of biaxial strain.

tric stress coefficients e_{ij}^{2D} have been renormalized by the length of unit cell along z direction (Lz): $C_{ij}^{2D} = Lz C_{ij}^{3D}$ and $e_{ij}^{2D} = Lz e_{ij}^{3D}$.

III. SYMMETRY ANALYSIS

The relaxed-ion piezoelectric stress tensors e_{ijk} and strain tensor d_{ijk} , from the sum of ionic and electronic contributions, is defined as:

$$e_{ijk} = \frac{\partial P_i}{\partial \varepsilon_{jk}} = e_{ijk}^{elc} + e_{ijk}^{ion} \quad (1)$$

and

$$d_{ijk} = \frac{\partial P_i}{\partial \sigma_{jk}} = d_{ijk}^{elc} + d_{ijk}^{ion} \quad (2)$$

where P_i , ε_{jk} and σ_{jk} are polarization vector, strain and stress, respectively. The d_{ijk} and e_{ijk} are related via the elastic stiffness tensor C_{ijkl} . Monolayer XSi_2N_4 belongs to the $\bar{6}m2$ point group. Employing the Voigt notation, if we only consider in-plane strain components^{6,11-14} for 2D materials, the e_{ij} , d_{ij} and C_{ij} become into:

$$\begin{pmatrix} e_{11} & -e_{11} & 0 \\ 0 & 0 & -e_{11} \\ 0 & 0 & 0 \end{pmatrix} \quad (3)$$

$$\begin{pmatrix} d_{11} & -d_{11} & 0 \\ 0 & 0 & -2d_{11} \\ 0 & 0 & 0 \end{pmatrix} \quad (4)$$

$$\begin{pmatrix} C_{11} & C_{12} & 0 \\ C_{12} & C_{11} & 0 \\ 0 & 0 & \frac{C_{11}-C_{12}}{2} \end{pmatrix} \quad (5)$$

Here, the only in-plane d_{11} is derived by $e_{ik} = d_{ij} C_{jk}$:

$$d_{11} = \frac{e_{11}}{C_{11} - C_{12}} \quad (6)$$

IV. MAIN CALCULATED RESULTS

The geometric structures of the XSi_2N_4 monolayer are plotted in Figure 1, which consist of seven atomic layers of N-Si-N-X-N-Si-N (a XN_2 layer sandwiched between two Si-N bilayers). The optimized structural parameters of XSi_2N_4 ($\text{X}=\text{Ti}, \text{Zr}, \text{Hf}, \text{Cr}, \text{Mo}$ and W) (in Table I) agree well with the previous calculated results¹⁸. The electronic band structures of these monolayers are also calculated using GGA and GGA+SOC, and the representative HfSi_2N_4 and WSi_2N_4 monolayers are shown in Figure 2. The energy bands of XSi_2N_4 ($\text{X}=\text{Ti}, \text{Zr}, \text{Cr}, \text{Mo}$) are plotted in Fig.1 and Fig.2 of supplementary materials. Compared to XSi_2N_4 ($\text{X}=\text{Ti}, \text{Zr}, \text{Hf}$), additional two electrons are added for XSi_2N_4 ($\text{X}=\text{Cr}, \text{Mo}$ and W), and then the first two conduction bands are filled. Their corresponding gaps (GGA and GGA+SOC) and spin-orbital splitting at K point are summarized in Table I. It is clearly seen that the difference of gap between GGA and GGA+SOC is very little. Calculated results show that the magnitude of spin-orbital splitting accords with the atomic mass of X.

Due to hexagonal symmetry, the two independent elastic stiffness coefficients (C_{11} and C_{12}) are calculated by SSR, and all calculated elastic coefficients satisfy the Born stability criteria²⁵. The elastic stiffness coefficients

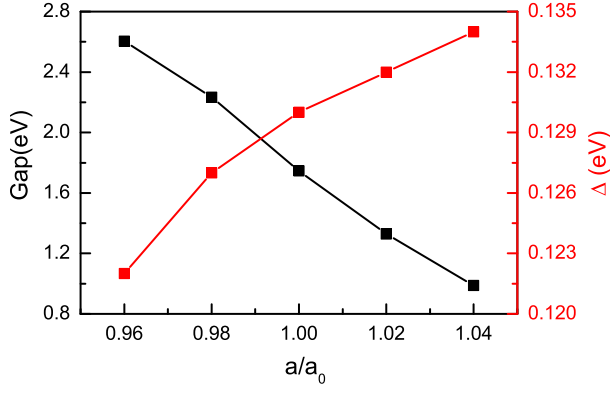


FIG. 5. (Color online) For experimentally achieved monolayer MoSi_2N_4 , the GGA+SOC gap and spin-orbital splitting at K point as a function of biaxial strain.

(C_{11} , C_{12} and $C_{11}-C_{12}$) are shown in Figure 3. These elastic constants are larger than ones of most 2D materials, like TMD, metal oxides, and III-V semiconductor materials^{11,13}, indicating that these 2D monolayers are more rigid than other 2D materials. The piezoelectric stress coefficients e_{11} of XSi_2N_4 monolayer are calculated by DFPT, using the rectangle supercell. Based on Equation 6, the piezoelectric strain coefficients d_{11} are attained. The piezoelectric coefficients e_{11} and d_{11} , and the ionic contribution and electronic contribution to e_{11} are plotted in Figure 3. Some key data are also listed in Table I. For all six monolayers, it is clearly seen that the ionic contribution and electronic contribution to e_{11} is opposite. The entire range of calculated e_{11} is from 2.229×10^{-10} C/m to 4.442×10^{-10} C/m, while the d_{11} ranges from 0.777 pm/V to 1.241 pm/V. Their d_{11} are smaller than ones of TMD monolayers (2.12 pm/V to 13.45 pm/V)^{11,13}. For example, the e_{11} of CrSi_2N_4 (4.442×10^{-10} C/m) and MoSi_2N_4 (4.398×10^{-10} C/m) are larger than one of MoS_2 (3.64×10^{-10} C/m), but their d_{11} (1.241 pm/V and 1.145 pm/V) are smaller than one of MoS_2 (3.73 pm/V)^{11,13}, which is due to larger $C_{11}-C_{12}$. Among all studied six monolayers, the CrSi_2N_4 monolayer has the best d_{11} .

The d_{11} of XSi_2N_4 monolayer is very small, and strain engineering is proposed to enhance their piezoelectric properties, which has been proved to a very effective way^{7,16,17}. Here, we use experimentally synthesized MoSi_2N_4 as an example to study the strain effects on piezoelectric properties. Due to $\bar{6}m2$ symmetry, biaxial strain can not induce polarization, not like uniaxial strain. We only consider biaxial strain effects on piezoelectric properties of MoSi_2N_4 , and the elastic constants $C_{11}-C_{12}$, piezoelectric coefficients e_{11} and d_{11} , and the ionic contribution and electronic contribution to e_{11} of monolayer MoSi_2N_4 as a function of biaxial strain are plotted in Figure 4. When the strain varies from -4% to 4%, the $C_{11}-C_{12}$ decreases, and the e_{11} increases, which gives rise to improved d_{11} based on Equation 6. At 4% strain, the d_{11} is 2.375 pm/V, which is more than twice

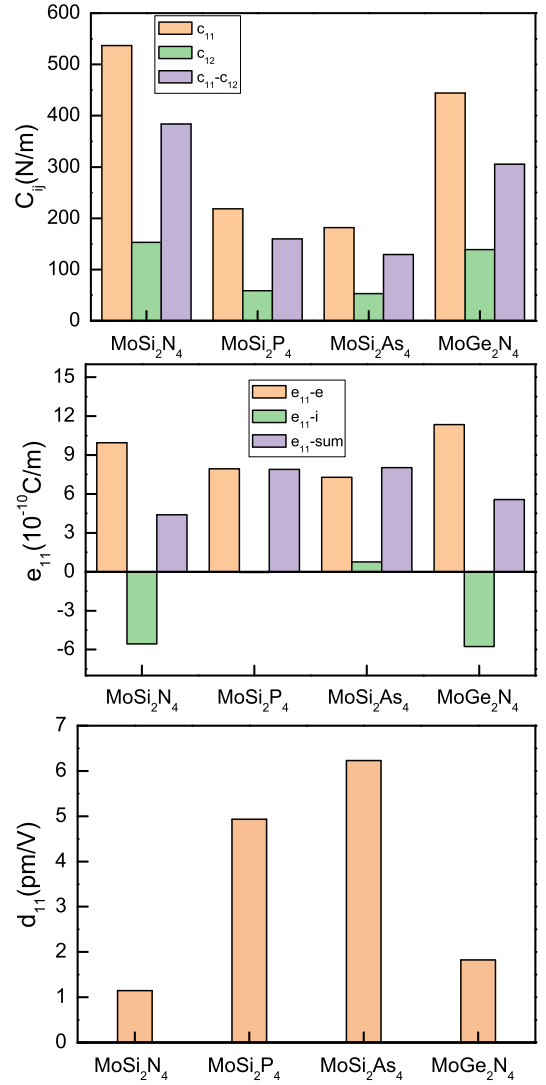


FIG. 6. (Color online) For monolayer MoSi_2N_4 , MoSi_2P_4 , MoSi_2As_4 and MoGe_2N_4 : (Top) the elastic constants C_{ij} , (Middle) piezoelectric stress coefficients e_{11} and the ionic contribution and electronic contribution to e_{11} , and (Bottom) piezoelectric strain coefficients d_{11} .

as large as unstrained one (1.145 pm/V). Similar biaxial strain-improved d_{11} can be found in monolayer $\text{g-C}_3\text{N}_4$ and MoS_2 ²⁶. It is found that both ionic contribution and electronic contribution to e_{11} have positive influence to improve d_{11} of monolayer MoSi_2N_4 , which is different from monolayer $\text{g-C}_3\text{N}_4$ and MoS_2 ²⁶.

At applied strain, the monolayer MoSi_2N_4 exhibits piezoelectricity, which should have a band gap. The gap and spin-orbital splitting Δ at K point as a function of strain are plotted in Figure 5, and the strain-related energy bands of MoSi_2N_4 are plotted in Fig.3 of supplementary materials. It is found that the gap decreases from 2.605 eV (-4%) to 0.988 eV (4%), while the Δ increases from 0.122 eV to 0.134 eV. The position of conduction band minimum (CBM) do not change from

-4% to 4%, but the position of valence band maximum (VBM) changes from K point to Γ point. The valence bands convergence can be observed at about -2% strain due to almost the same energy between K point and Γ point, which is in favour of better p-type Seebeck coefficient. Similar strain-induced bands convergence can be observed in many 2D materials like PtSe₂²⁷.

To further enhance piezoelectric properties, using elements of group IVA and elements of group VA to replace the Si and N elements in experimentally synthesized MoSi₂N₄, the monolayer MoSi₂P₄, MoSi₂As₄ and MoGe₂N₄ are proved to be stable¹⁸. The elastic constants C_{11} - C_{12} , piezoelectric coefficients e_{11} and d_{11} , and the ionic contribution and electronic contribution to e_{11} of monolayer MoSi₂N₄, MoSi₂P₄, MoSi₂As₄ and MoGe₂N₄ are plotted in Figure 6. It is clearly seen that monolayer MoSi₂P₄ and MoSi₂As₄ have very higher d_{11} than MoSi₂N₄, and they are 4.93 pm/V and 6.23 pm/V, which are comparable to one of most TMD monolayers¹¹. One reason of the high d_{11} for monolayer MoSi₂P₄ and MoSi₂As₄ is that monolayer MoSi₂P₄ and MoSi₂As₄ have more smaller C_{11} and C_{12} than MoSi₂N₄, which leads to smaller C_{11} - C_{12} . Another reason is that the minus of the ionic contribution to e_{11} of monolayer MoSi₂P₄ is very small, and the ionic contribution is positive for monolayer MoSi₂As₄. The d_{11} of monolayer MoGe₂N₄ is 1.83 pm/V. which is close to one of MoSi₂N₄.

V. CONCLUSION

Significant progress has been achieved in synthesizing monolayer MoSi₂N₄ with a non-centrosymmetric struc-

ture, which allows it to be piezoelectric. Here, the piezoelectric properties of monolayer XSi₂N₄ (X=Ti, Zr, Hf, Cr, Mo and W) are studied by using first-principles calculations. In the considered six materials, the CrSi₂N₄ is predicted to have the best d_{11} of 1.24 pm/V, and the second is 1.15 pm/V for experimentally synthesized MoSi₂N₄. It is found that strain engineering can improve d_{11} of MoSi₂N₄, and the d_{11} at 4% biaxial strain can improve by 107%. Compared to monolayer XSi₂N₄ (X=Ti, Zr, Hf, Cr, Mo and W), the monolayer MoSi₂P₄, MoSi₂As₄ and MoGe₂N₄ have more higher d_{11} , and the d_{11} of MoSi₂As₄ is as high as 6.23 pm/V. Owing to the recent CVD growth in monolayer MoSi₂N₄, it is expected that these monolayers XY₂M₄ (X=Ti, Zr, Hf, Cr, Mo or W; Y=Si or Ge; and M=N, P or As) may be put to a wide practical piezoelectric use in the future.

ACKNOWLEDGMENTS

This work is supported by the Natural Science Foundation of Shaanxi Provincial Department of Education (19JK0809). We are grateful to the Advanced Analysis and Computation Center of China University of Mining and Technology (CUMT) for the award of CPU hours and WIEN2k/VASP software to accomplish this work.

-
- ¹ W. Wu and Z. L. Wang, Nat. Rev. Mater. **1**, 16031 (2016).
 - ² W. Wu, L. Wang, Y. Li, F. Zhang, L. Lin, S. Niu, D. Chenet, X. Zhang, Y. Hao, T. F. Heinz, J. Hone and Z. L. Wang, Nature **514**, 470 (2014).
 - ³ H. Zhu, Y. Wang, J. Xiao, M. Liu, S. Xiong, Z. J. Wong, Z. Ye, Y. Ye, X. Yin and X. Zhang, Nat. Nanotechnol. **10**, 151 (2015).
 - ⁴ A. Y. Lu, H. Zhu, J. Xiao, C. P. Chuu, Y. Han, M. H. Chiu, C. C. Cheng, C. W. Yang, K. H. Wei, Y. Yang, Y. Wang, D. Sokaras, D. Nordlund, P. Yang, D. A. Muller, M. Y. Chou, X. Zhang and L. J. Li, Nat. Nanotechnol. **12**, 744 (2017).
 - ⁵ M. Dai, Z. Wang, F. Wang, Y. Qiu, J. Zhang, C. Y. Xu, T. Zhai, W. Cao, Y. Fu, D. Jia, Y. Zhou, and P. A. Hu, Nano Lett. **19**, 5416 (2019).
 - ⁶ L. Dong, J. Lou and V. B. Shenoy, ACS Nano, **11**, 8242 (2017).
 - ⁷ S. D. Guo, X. S. Guo, Y. Y. Zhang and K. Luo, J. Alloy. Compd. **822**, 153577 (2020).
 - ⁸ Y. Xu, Z. Q. Li, C. Y. He, J. Li, T. Ouyang, C. X. Zhang, C. Tang and J. X. Zhong Appl. Phys. Lett. **116**, 023103 (2020).
 - ⁹ S. D. Guo, X. S. Guo, Z. Y. Liu and Y. N. Quan, J. Appl. Phys. **127**, 064302 (2020).
 - ¹⁰ S. D. Guo and S. Q. Wang, J. Phys. Chem. Solids **140**, 109375 (2020).
 - ¹¹ M. N. Blonsky, H. L. Zhuang, A. K. Singh and R. G. Hennig, ACS Nano, **9**, 9885 (2015).
 - ¹² R. X. Fei, We. B. Li, J. Li and L. Yang, Appl. Phys. Lett. **107**, 173104 (2015)
 - ¹³ K. N. Duerloo, M. T. Ong and E. J. Reed, J. Phys. Chem. Lett. **3**, 2871 (2012).
 - ¹⁴ Y. Chen, J. Y. Liu, J. B. Yu, Y. G. Guo and Q. Sun, Phys. Chem. Chem. Phys. **21**, 1207 (2019).
 - ¹⁵ Y. G. Guo, H. Q. Zhu and Q. Wang, ACS Appl. Mater. Interfaces **11**, 1033 (2019).
 - ¹⁶ N. Jena, Dimple, S. D. Behere and A. D. Sarkar, J. Phys. Chem. C **121**, 9181 (2017).
 - ¹⁷ Dimple, N. Jena, A. Rawat, R. Ahammed, M. K. Mohanta and A. D. Sarkar, J. Mater. Chem. A **6**, 24885 (2018).
 - ¹⁸ Y. L. Hong, Z. B. Liu, L. Wang et al., Science **369**, 670 (2020).
 - ¹⁹ X. Wu, D. Vanderbilt and D. R. Hamann, Phys. Rev. B **72**, 035105 (2005).

- ²⁰ P. Hohenberg and W. Kohn, Phys. Rev. **136**, B864 (1964);
W. Kohn and L. J. Sham, Phys. Rev. **140**, A1133 (1965).
- ²¹ G. Kresse, J. Non-Cryst. Solids **193**, 222 (1995).
- ²² G. Kresse and J. Furthmüller, Comput. Mater. Sci. **6**, **15** (1996).
- ²³ G. Kresse and D. Joubert, Phys. Rev. B **59**, 1758 (1999).
- ²⁴ J. P. Perdew, K. Burke and M. Ernzerhof, Phys. Rev. Lett. **77**, 3865 (1996).
- ²⁵ R. C. Andrew, R. E. Mapasha, A. M. Ukpong and N. Chetty, Phys. Rev. B **85**, 125428 (2012).
- ²⁶ S. D. Guo, W. Q. Mu and Y. T. Zhu, in preparation.
- ²⁷ S. D. Guo, J. Mater. Chem. C, **4**, 9366 (2016).